Amorphous Dielectric Optical Coatings Deposited by Plasma Ion Assisted Electron Beam Evaporation for Gravitational Wave Detectors

Carlos Garcia Nuñez[1*], Gavin Wallace[2], Lewis Fleming[1], Kieran Craig[2], Shigeng Song[1,5], Sam Ahmadzadeh[1], Caspar Clark[3,1], Simon Tait[4], Iain Martin[4], Stuart Reid[2], Sheila Rowan[4], Des Gibson[1,5]

[1]*Institute of Thin Films, Sensors and Imaging, University of the West of Scotland, SUPA, Paisley PA1 2BE, Scotland, UK*
[2]*University of Strathclyde, SUPA Glasgow G1 1XQ, Scotland, UK*
[3]*Helia Photonics Ltd, Rosebank Park, Livingston West Lothian EH54 7EJ, Scotland, UK*
[4]*University of Glasgow, SUPA Glasgow G12 8QQ, Scotland, UK*
[5]*Albasense Ltd, Paisley PA1 2BE, Scotland, UK*
**carlos.garcianunez@uws.ac.uk*

Abstract: Coating thermal noise (CTN) in amorphous coatings is a drawback hindering their application in precision experiments such as gravitational wave detectors (GWDs). Mirrors for GWDs are Bragg's reflectors consisting of a bilayer-based stack of high and low refractive index materials showing high reflectivity and low CTN. In this paper, we report the characterisation of morphological, structural, optical, and mechanical properties of high index materials such as scandia (Sc_2O_3) and hafnia (HfO_2) and a low index material such as magnesium fluoride (MgF_2) deposited by plasma ion-assisted electron beam evaporation. We also evaluate their properties under different annealing treatments and discuss their potential for GWDs.

1. Introduction

Optical interference coatings for gravitational wave detection have to meet a variety of specific requirements, such as low absorption, high reflectance and low mechanical losses, as well as high resistance against damage by power laser radiation, and long-term optical stability [1]. When utilised in gravitational wave detectors (GWDs), material processing for coatings on large and massive suspended mirrors leads to additional problems arising from the requirements of low stress, low density of defects and high uniformity. To that end, the improvement of more reliable and sophisticated thin-film deposition technologies is needed, allowing next generation of GWDs to augment their sensitivity towards the detection of interacting black holes, neutron stars, and even new unpredicted phenomena [2].

High reflecting (HR) coatings utilised in GWDs such as Advanced LIGO, Advanced Virgo and KAGRA consist of Bragg's reflectors alternating layers of low (SiO_2, $1.44 < n < 1.48$ at $\lambda = 1064$ nm) and high (TiO_2:Ta_2O_5, $n = 2.11$ at $\lambda = 1064$ nm) refractive-index materials and are typically deposited by ion-beam sputtering (IBS) techniques [3]. Reflectivities as high as R > 99.9995% can be achieved with coating mechanical losses of $(2.4.0\pm0.1)\times10^{-4}$ rad (annealed TiO_2:Ta_2O_5, with Ti/Ta =0.27 optimal ratio) to $(4.5\pm0.3)\times10^{-5}$ rad (SiO_2) in the band of 50 to 900 Hz [3], and optical absorption of less than 0.5 ppm (at $\lambda = 1064$ nm) [4], [5]. Moreover, in this advanced GWDs, coating uniformity on a large scale (better than 99.9% over Ø15 cm diameter) is required [5]. IBS system at LMA has demonstrated great results on Ti-Ta_2O_5/SiO_2

HR coatings, thanks to the use of a sample holder with a planetary motion coupled with a dedicated mask, exhibiting uniformities above 99.8% on Ø16 cm in monolayers, and above 99.95% in HR coatings on Ø24 cm [5]. However, IBS suffers main drawbacks being the unintentional incorporation of Ar bubbles [6][7] and the excessive oxygen entrapped in the nanobubbles observed in oxide-based films [8], during the deposition process [6] and after annealing processes [9], hindering the optical and mechanical properties of the coating [10][11]. IBS deposition rates are highly influenced by growth parameters (source settings, reactive atmosphere pressure, bombardment, etc.) showing values ranged between 0.01 nm/s (e.g., for IBS HfO_2) [12] or 0.1 nm/s (e.g., for IBS MgF_2) [13]. The deposition rates achieved by alternative techniques such as reactive biased target deposition (RBTD) are around an order of magnitude lower than with a gridded IBS system, exhibiting growth rates around 0.0096 nm/s for Sc_2O_3 [14]. Alternative deposition techniques such as plasma ion assisted electron beam evaporation (PA-EBE) offers the possibility to deposit high quality films preventing the utilisation of Ar (avoiding unwanted bubbles) increasing the deposition rates up to 0.3 nm/s (this work). In this regard, optimisation of the coating design aiming to dilute the loss contribution of the high-index material has been explored through the deposition of new materials and utilisation of deposition techniques different to IBS. The latter includes techniques such as PA-EBE [15], [16], highly promising for producing highly uniform coatings at higher deposition rates than IBS (factor 10) and greatly scalable (needed for the fabrication of mirrors at main GWDs).

Scandium sesquioxide (Sc_2O_3) or also known as *scandia* is a high refractive index material who has been presented as a promising material for its use in optical interference coatings in GWDs and other high-power lasers applications (e.g., high power remove laser transmission and optoelectronic functional devices) [17][18], mainly due to its high bandgap (5.7 eV) [19], which is larger than other high index metal-oxides like HfO_2[20]. Since the theory predicts that the scaling of the laser breakdown fluence with the bandgap, and the utilisation of a dielectric material with a wider band gap energy will prevent laser damage in aforementioned applications [20]. Along with low index materials such as SiO_2, though not widely studied, Sc_2O_3 has been demonstrated in dielectric interference-based mirror coatings developed for high-power ultraviolet (UV) lasers [21]. High optical coatings based on Sc_2O_3 have been successfully deposited by techniques, including IBS [22], [23], reactive magnetron sputtering (RMS) [24], pulsed laser deposition (PLD)[25], and reactive biased target sputtering deposition (RBTD) [14].

Hafnium dioxide (HfO_2) also called *hafnia*, is a dielectric material characterized by a high refractive index, exhibiting a large laser damage threshold [26] due to a wide bandgap energy of around 5.5 eV [27]. As a result of these properties and its transparency over a wide range in the electromagnetic spectrum, covering from the UV to the mid-IR, is widely utilised in optical coating applications [28] and investigated as promising material GWDs [12]. In contrast to Sc_2O_3, the optical properties of HfO_2 have been extensively studied, however, these studies have offered a variety of conclusions regarding the refractive index and the extinction coefficient [29], [30]. This large scattering of optical constants is originated mainly from the use of different techniques. Among all, both ion-assisted electron beam evaporation and sputtering presented the more compact films with refractive index close to those reported for bulk HfO_2 [31], while electron-beam evaporated films demonstrated to have lower refractive index values [32]. This material has been also deposited by atomic layer deposition (ALD) [33][34] RMS [35], and IBS, the latter being characterised at cryogenic conditions, for future GWDs such as Einstein Telescope [36]. In those characterisations, HfO_2 presented extremely low loss angles ($2\text{-}3\times10^{-4}$) but with Young's modulus values four times higher than that obtained in low-index materials such as SiO_2. This dissimilarity found in the Young's modulus values between substrate (SiO_2) and coating based on HfO_2 lead to increased thermal noise.

Fluoride thin films such as magnesium fluoride (MgF_2) are widely used for a wide number of optical applications due to their beneficial characteristics, including a relatively high damage

threshold (useful for high power lasers applications), high hardness, good stability in hostile environments, and a very low refractive index (n = 1.38) [37]. However, MgF_2 films deposited by means of IBS [13], RMS[38], ion beam assisted deposition (IBAD) and vacuum evaporation techniques at room temperature, the latter resulting in porous columnar microstructure [39]. That is a drawback for mirror coatings since the porous tend to be filled by moisture in room air leading to a detrimental effect on the stability of the coatings through the variation of the optical and mechanical properties of the coating.

This work presents a study of optical and mechanical properties of three potential material candidates to improve the performance of next generation of GWDs, including scandium oxide (Sc_2O_3, scandia), magnesium fluoride (MgF_2, sellaite) and hafnium oxide (HfO_2, hafnia). These films were deposited by PA-EBE which is a technique that presents some advantages with respect to standard IBS, including less or zero Ar-gas impurities and material consumption [40]. Moreover, PA-EBE also presents high deposition rates (0.3 nm/s, factor 10 higher than IBS), great thickness control and radial uniformity (in this work: 99.98% uniformity over Ø10.16 cm coatings) being essential for the coating of large test mass in GWDs. PA-EBE also has a good control on the doping through the utilisation of multiple crucibles to control the material mixing during the so-called co-deposition. Good examples of that accurate doping control are metal oxide films, e.g., 0.5-2wt% in doped titanium oxide [41] and 0.6-5wt% in doped indium oxides [42].

2. Experimental details

2.1 Deposition of thin films

Single layer coatings consisting of 396-nm thick Sc_2O_3, 345-nm thick MgF_2 and 238-nm thick HfO_2 were deposited using plasma ion assisted electron beam evaporation (Satis 1200), being a vacuum deposition system with a multi-pocket Temescal electron beam gun (Fig. 1). This work utilizes a novel plasma source based on inductive heating inner and outer surfaces of a lanthanum hexaboride high-efficiency thermionic emitter hollow cathode [43]. In the case of MgF_2 films, 1-3 mm pellets (99.99% purity) were utilised. For the deposition of metal oxides, 5-mm drops of Hf with a purity of 99.5%, and 2-mm granules of Sc_2O_3 with a purity of 99.99% were loaded in a crucible at the PA-EBE system, for their later evaporation using an electron beam (Part 8 in Fig. 1), and oxidized with an oxygen plasma source (Part 7 in Fig. 1).

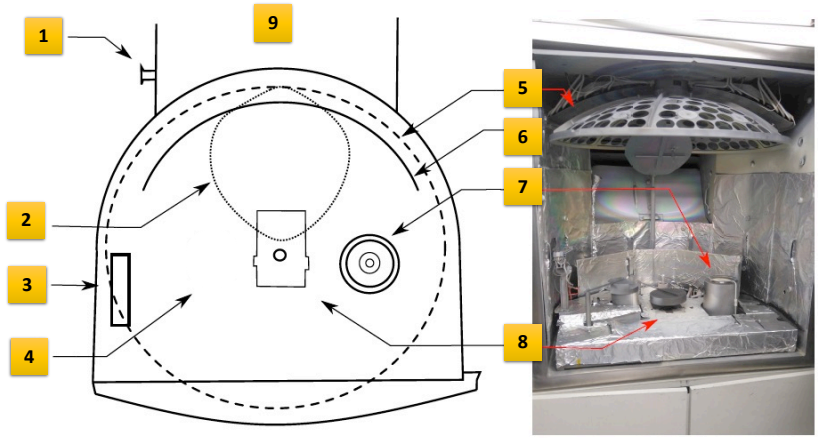

Fig. 1. Schematic (left) and front view photo (right) of the PA-EBE system used in this work. PA-EBE key parts consist of: (1) characterisation port; (2) uniformity mask; (3) quartz heater; (4) deposition/main chamber; (5) calotte; (6) Meissner trap; (7) Thin Film Solutions plasma source; (8) electron beam gun; (9) vacuum pump port.

The deposition conditions were optimised using design of experiments (DoE) to determine not only the influence of the growth parameters on the growth rate, but also to find a low deposition rate (thickness control) producing good optical properties (i.e., high n and low k). The studied deposition parameters comprised the accelerating current (I_{AC}), accelerating volage (V_{AC}), external current (I_{EX}), O_2 flux, Ar flux at the cathode ($Ar_{Cathode}$), Ar flux at the anode (Ar_{Anode}), and the induction power heater. Table 1 summarises the optimised deposition conditions for each coating, as well as resulting e-beam evaporation rates.

Table 1. PA-EBE experimental conditions used to deposit Sc_2O_3, HfO_2 and MgF_2 coatings.

Material	I_{AC} (A)	V_{AC} (V)	I_{EX} (A)	Glass flow (sccm)			Induction power heater (kW)	e-beam evap. rate (Å/s)
				O_2	Ar Cathode	Ar Anode		
Sc_2O_3	43	140	10	97	6	6	1.5	1
HfO_2	43	140	10	97	7	7	1.5	0.7
MgF_2	43	130	10	-	7	7	1.5	15

2.2 Characterisation of thin films

Morphological properties of the coatings, including thickness, pinholes density and surface roughness, were analysed by scanning electron microscopy (SEM) at 20 kV (S4100 cold FEG from Hitachi). The amorphous structure of the films was also analysed by grazing-incidence X-ray diffraction (GIXRD) analysis (Siemens D5000, Cu Kα radiation at 40 kV/30 mA). Films composition (i.e., stoichiometry) was analysed by energy dispersive X-ray (EDX) analysis (S4100 cold FEG from Hitachi).

Optical properties of coatings, including refractive index (n) and extinction coefficient (k) as well as a confirmation of films thickness (d) have been obtained by spectrophotometry (UV-VIS-IR spectrophotometer from Aquila Instruments) with a resolution for the extinction

coefficient of 10^{-3}. For this, films were deposited on glass slides (JGS3) for transmission measurements and Si(100) substrates for reflection measurements. Prior to the deposition, Si substrates were cleaned in an ultrasound bath (5 min acetone, followed by 5 min IPA) rinsed in DI water and dried under nitrogen flow. Glass substrates were cleaned in an automatic cleaning system, where they were subsequently dipped in different baths, consisting of acid solution, base solution, DI water (with ultrasounds), and DI water (hot water + slow pulling mechanism). Optical density (OD) was measured as a function of the wavelength (λ) at experimental conditions, comprising incident angle of 0°, P polarisation, and tolerance of 0.5%. Then, MacLeod software was utilised to calculate n, k and d of each coating by fitting the experimental data to a single layer model. Then, Sellmeier expression was used to represent n as a function of the wavelength.

Stress measurements were carried out in a Wafer Geometry Gauge system (MX 203-6-33 from E+H Metrology GmbH). 4-inch Si(100) wafers (also called here discs) with a thickness of 0.1 mm were used as substrates. The gauge is a manually loaded wafer geometry measuring instrument for round wafers (mainly silicon wafers, but open to other materials as well). This equipment is dedicated to control the thickness and shape of wafers, as well as evaluation of the average stress calculated from the local stress measured across the wafer, key for this work. E+H Metrology system, like other wafer geometry instruments, uses a contactless capacitive distance sensor to determine aforementioned parameters (see more details in Section A of Supplementary information). The MX-NT and Wafer Studio software were used to carry out the measurements and for the visualization and data analysis, respectively. Fig. 2 shows the calculation of stress from pre-measurements and post measurements carried out in a blank disc and a coated disc, respectively. Coating stress varies across the area of the coating which is known as the local stress which is influenced by material type and deposition method. Factors such as orientation of the wafer in the coating chamber, substrate rotation, reactive gas angle of delivery and other process parameters can all effect the local stress values and will result in a deviation from radial symmetry. In addition, the irregular starting geometry of a wafer will also mean that a perfect radial symmetry in local coating stress is unlikely to be observed. The local the local stress represented in Fig. 2(b) has symmetry across the y-axis and a separate symmetry across the x-axis. This symmetry mirrors the local thickness deviation of the wafer which is represented in Fig. 2(a) so it is a reasonable assumption to make, that the main contributing factor to local stress variation is from the local thickness variation inherent to the coated wafer.

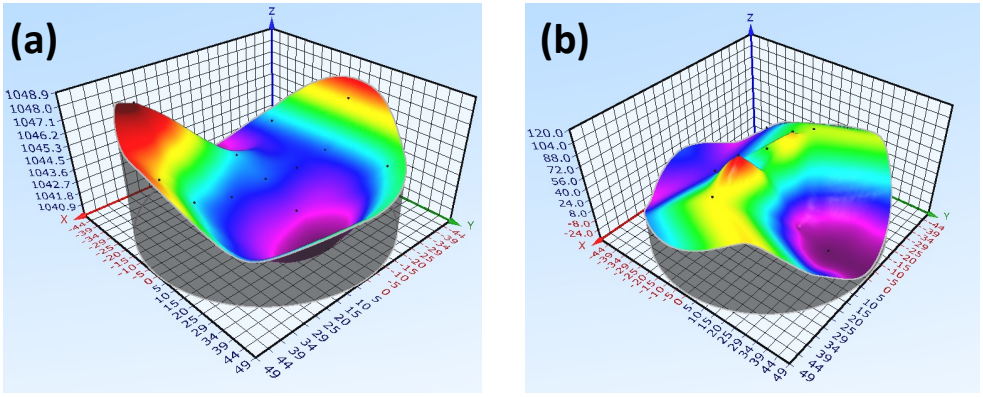

Fig. 2. Visualisation of (a) the blank disc local thickness expressed in µm units, measured prior to the coating deposition (*pre-measurement*), and (b) the Sc_2O_3 coating on Si wafer local stress (from which the average stress value is derived) expressed in MPa (*post-measurement*).

Photo-thermal common-path interferometry referred here as PCI [44], has been used for thermally based absorption measurements at 1064 nm and with an accuracy of less than 1 part per million (ppm), allowing measurement of the weak coating absorption and determine their extinction coefficient. As it will be thoroughly described later on in Table 5, the three materials investigated here are expected to exhibit optical absorptions above 10 ppm [45] [46]. For these measurements, coatings were deposited on glass disc substrates (Corning 7980) with a thickness of 6 mm and a diameter of 1 inch. Each of the measures are the average of 10 points taken across the surface of the samples, where the resultant error on the absorption is indicative of the level of spread between point-to-point across the coating surface. This method was used to obtain both the coating absorption expressed in ppm units and the extinction coefficient (k).

Q-factor measurements were carried out to obtain the mechanical loss angle (ϕ) of each coating with coatings deposited on fused silica substrates (SiO_2, double side polished [DSP], with flat, Corning 7980 from University Wafers) with a diameter of 3-inch, thickness of 511±1μm and a flat of 25 mm. Prior to the deposition, substrates were pre-annealed at 1000ºC for 4 hours in order to remove any mechanical stress accumulated in the structure of the substrate during both manufacturing and transporting processes.

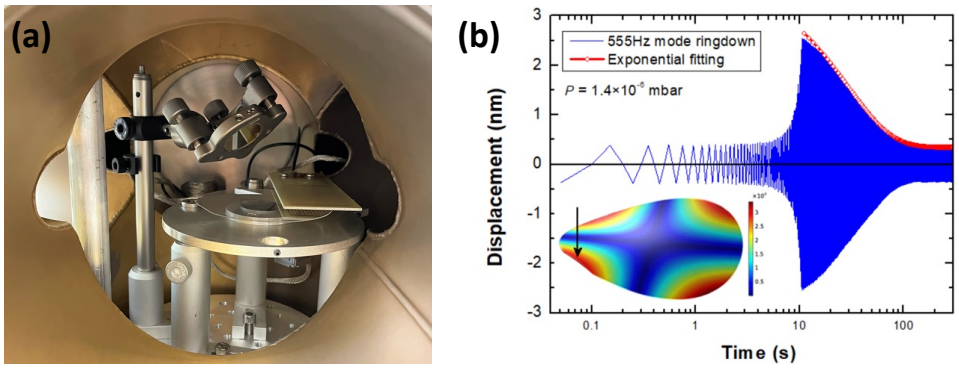

Fig. 3. (a) Photograph of the Gentle Node Suspension (GeNS) used to carry out the Q-factor measurements or the mechanical loss angle of the coatings. (b) Ringdown of the fundamental mode (555 Hz) of the substrate measured at $1.4\text{x}10^{-6}$ mbar to prevent damping effects; inset: FEM simulation of the resonant mode and the peripherical point under analysis.

The ϕ was measured using a GeNS placed inside a vacuum chamber (Fig. 3(a))[47], recording the decay of the sample excited resonant mode amplitude or ringdown (Fig. 3(b)), exhibiting damped harmonic motion, consisting of carrier and envelope signals, where the amplitude of the envelope is:

$$V(t) = V_0 \exp[-\pi f_0 \phi(f_0) t] \quad (1)$$

Where V_0 is the amplitude of the signal measured by the QPD over time, f_0 is the resonant frequency pre-found by FEA (and later confirmed by using a spectrum analyser). From (1), fitting of the ringdown measurement allows direct calculation of the mechanical loss angle as a function of the resonant mode frequency. The coating loss (ϕ_{coating} coating) is

$$\phi(f_0)_{\text{coating}} = \frac{E_s}{E_c}[\phi(f_0)_{\text{coated}} - \phi(f_0)_{\text{substrate}}] \quad (2)$$

where E_s/E_c is the substrate/coating energy ratio estimated using finite elements analysis ANSYS package (Workbench 2021 Development R2) and utilised here to calculate ϕ_{coating} by Eq (2) for each of the resonant modes [48]. FEA method also allows to correct the initial Young's modulus of the coating by adjusting the position of the resonant frequency (f_0)

measured by the spectrum analyser to that obtained by the simulation [49]. For these simulations, Poisson ratio (ν), Young's modulus, coating density, and coefficient of thermal expansion (CTE) have been used. The values of these magnitudes could be found in Section B of Supplementary Material. The ringdown measurements of the substrates, and the coated substrates were repeated 5 times. This process has been automatised using LabVIEW, allowing to carry out multiple measurements at different resonant modes. Since each mode typically requires the use of a different excitation AC signal (AC voltage and offset voltage) applied to the excitation plate, this program drastically reduces the measurement time, and optimises the acquisition and interpretation of the data. The program also estimates both the time constant of the exponential decay measured from each ringdown measurement and the resulting mechanical loss angle. The error analysis is further described in Section D of Supplementary Material.

Annealing of the samples was carried out in a Carbolite Furnace (CSF 1200) at temperatures ranged between 100ºC and 700 ºC, in order to study the effects on the stress values, optical properties (i.e., refractive index) and the mechanical loss angle.

3. Results and discussion

3.1 Morphological characterisation

A visual inspection of the coatings deposited by plasma ion assisted electron beam evaporation on a 4-inch Si(100) wafer showed a uniform film over the large area of the substrate (Fig. 4(a)). SEM analysis of the films demonstrated an amorphous morphology in the three materials under study (Fig. 4(b-d)). These results are in good agreement with those obtained by XRD analysis (*see* diffractograms in the next section). Moreover, the analysis of the coatings by optical microscopy also confirmed the absence of pinholes in the resulting films, making these coatings to be presented as a great candidate for high reflecting mirrors. SEM images of the film cross section (Fig. 4(e-g)) probed the high uniformity achieved over large areas (wafer scale) during the PA-EBE deposition of the films. Coating uniformity was evaluated by mapping the large area of the 4-inch coated wafer, analysing the cross-section of 12 different points of the wafer (*see* Section C in Supplementary Material). Results conclude a variation of that thickness below 0.03% (HfO_2), 0.02% (MgF_2) and 0.02% (Sc_2O_3), meaning a thickness uniformity above 99.97%, 99.98%, and 99.98%, for the HfO_2, MgF_2 and Sc_2O_3 coatings, respectively. Considering the requirement for future GWDs of thickness uniformities better than 99.9% over Ø15 cm diameter [5], these results make PA-EBE to be a promising technique for producing HR uniform coatings at wafer scale.

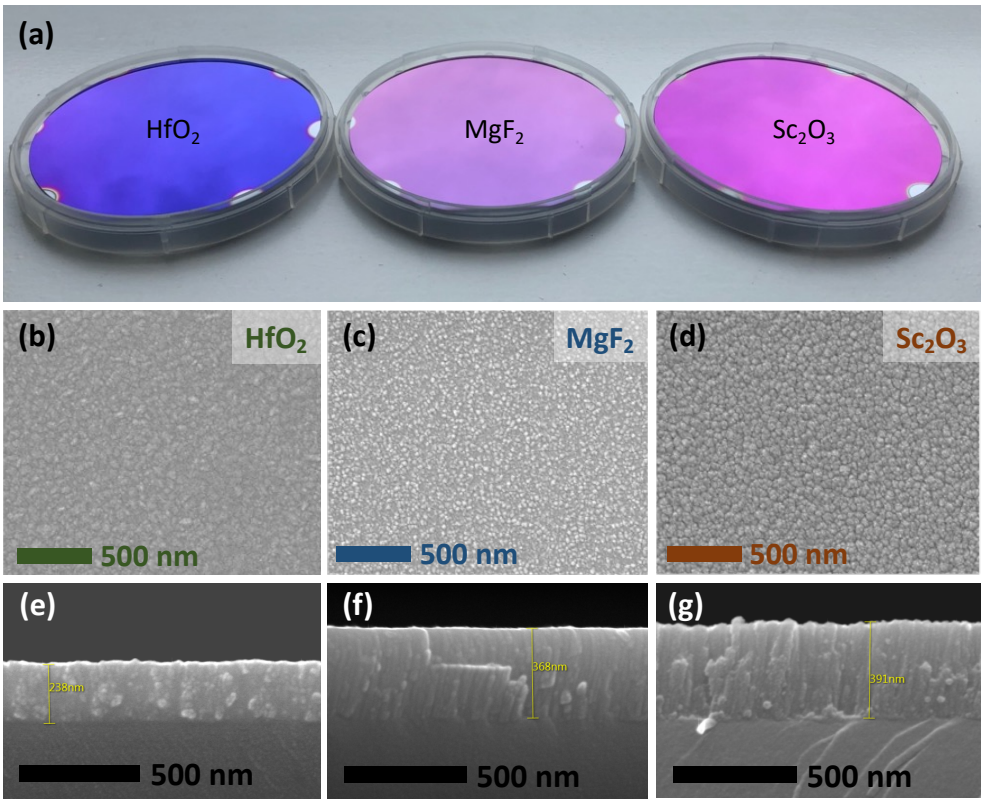

Fig. 4. (a) Photograph of the HfO_2 (*left*), MgF_2 (*middle*) and Sc_2O_3 (*right*) optical coatings deposited by plasma ion assisted electron beam evaporation. (b-d) Top and (e-g) cross section SEM images of the optical coatings.

3.2 Structural analysis

XRD analysis was used to characterise the structure of the films right after their deposition (Before Annealing, BA) and after annealing treatments carried out for 2 hours at different temperatures ranged between 100 and 700 °C. Fig. 5 (a-c) demonstrates highly amorphous films before the annealing treatment, in good agreement with SEM observations of the surface morphology (Fig. 4). To attribute the crystalline phase(s), the positions of Bragg peaks were compared to the International Centre for Diffraction Database (ICDD).

BA, Sc_2O_3 exhibited a broad peak centred around 31.561°, identified with a star (☆) in Fig. 5(a) which could correspond to the (222) diffraction plane in the Sc_2O_3 structure (ICDD card no. 00-005-0629) [50]. The large full width at half maximum (FWHM) of this peak evidenced the amorphous characteristic of the PA-EBE Sc_2O_3 film. This FWHM was observed not to be affected by the annealing temperature, in contrast to its intensity, whose value was increased by this treatment. This result indicated that some level of crystal order was produced by the thermal treatment and was greatly visible at temperatures above 400 °C. Fig. 5 (a) also showed other peaks labelled with circle (○) corresponding to the diffraction peaks from the Si substrate. This was confirmed by the characterisation of pristine Si(100) substrate in the same conditions (i.e., after the same thermal treatments).

BA, MgF_2 coating presented a peak centred around 28.76° (Fig. 5 (b)) which could correspond to the (110) diffraction of this material, and a second peak at 40.3° which could be originated

by the (111) diffraction plane (ICDD card no. 00-006-0290) [50]. This second peak could be embedded within a Si a diffraction peak. MgF_2 peaks in the figure are labelled with triangle (△). As in the case of Sc_2O_3, FWHM of these peaks showed no widening under thermal treatments, but a certain increase of their intensity for temperatures above 400 ºC.

Finally, HfO_2 BA showed four peaks (Fig. 5 (c)) whose intensity increased with the temperature, including 30.2º, 32.58º, 32.96º, and 39.62º, corresponding to (011), (120), (200), and (121), respectively (ICDD card no. 00-034-0104) [50]. The two peaks centred at 32.58º and 32.96º were only visible for annealing temperatures above 500 ºC, evidencing the partial crystallization of the film above those temperatures.

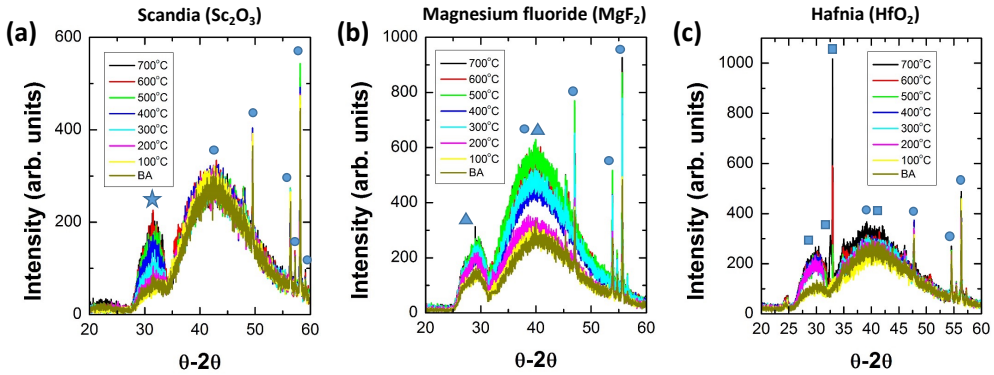

Fig. 5. GIXRD diffractograms of (a) Sc_2O_3 (b) MgF_2 and (c) HfO_2 films PA-EBE on Si(100) measured before annealing (BA) and after 2 hours annealings carried out in air ambient at 100, 200, 300, 400, 500, 600 and 700 ºC. Sc_2O_3 (star ☆), MgF_2 (triangle △), HfO_2 (square ▢) and Si (circle ○) diffraction peaks, have been labelled in the diffractograms.

3.3 Compositional study

Table 2 summarises the compositional analysis of the three coatings. The table provides the atomic ratio of each binary compound defined as A_xB_y, where A and B correspond to the cations and anions, respectively, and y/x is the anion to cation ratio. The stoichiometric column presents the ideal y/x for each of the compounds. For comparison, the table also shows the y/x obtained by other deposition techniques utilised to synthesize the sample three materials. From the comparison, it is observed that PA-EBE produced non-stoichiometric coatings, exhibiting oxygen excess in both hafnia and scandia (*over stoichiometric*), and fluor deficit in the magnesium fluoride coating (*under stoichiometric*). Compared to other techniques such as atomic layer deposition (ALD)[33], reactive magnetron sputtering (RMS) [35], IBS [36], and RBTD [12], exhibiting HfO_2 stoichiometric films (i.e., y/x of around 2.00), PA-EBE used in this work resulted in over stoichiometric films. Further depositions using design of experiments (DoE) will allow to determine the role of oxygen on the resulting film stoichiometry, and thus, to tune the stoichiometry of the coatings. Similarly, Sc_2O_3 films deposited in this work, presented a y/x value around 2.1, being above the stochiometric films achieved by ALD [33] [34], RMS [24], PLD[25], and RBTD [14]. In the case of MgF_2, the under stoichiometric values obtained here of 1.7 are slightly lower to those reported with EBE (1.95), but close to those obtained by RMS and IBS [13].

In spite of this drastic difference in the composition of the films did not affect the amorphous characteristics of the resulting coatings as demonstrated by SEM and XRD, however, it had a high impact on the mechanical and optical properties of the three materials as it will be presented later on.

Table 2. EDX analysis of optical coatings deposited by PA-EBE (*this work*) and other techniques.

Coating	Atomic ratio (y/x)		
	Stoichiometric film	This work	Other deposition techniques
Hf_xO_y	2.0	3.4	2.00 (ALD) [33] 1.96 (RMS) [35] 2.00 (RBTD) [12] 2.00 (IBS) [36]
Mg_xF_y	2.0	1.7	1.95 (EBE) [51] 1.95 (IBAD) [52] 1.90 (RMS) [38] 1.92 (IBS) [13]
Sc_xO_y	1.5	2.1	1.49-1.53 (ALD) [33] [34] 1.53 (RMS) [24] 1.52 (PLD)[25] 1.50 (IBS) [22], [23] 1.51 (RBTD) [14]

PLD: pulsed laser deposition; **ALD**: atomic layer deposition; **RMS**: reactive magnetron sputtering; **RBTD**: reactive biased target sputtering deposition; **IBS:** ion beam sputtering; **DE:** direct evaporation; **IBAD:** ion beam assisted deposition.

3.5 Stress measurements

The stress value obtained in Sc_2O_3 films around 32.19 MPa, indicates a tensile stress which is orders of magnitudes lower than those reported for IBS Sc_2O_3 films (range of GPa) the latter caused by the high density of oxygen interstitials produced by that Ar based IBS method [53]. MgF_2 films evaporated in this work exhibit 150 MPa. This result evidence a tensile stress lower than those reported in the literature (550 MPa)[54]. The origin of that stress reduction could be due to the benefits of plasma ion assisted method used here, contributing to decline the density of isolated crystalline aggregates, leading to the increase of the partial disorder in the resulting structure. Tensile stress values of 118 MPa obtained for HfO_2 are in good agreement with the 115 MPa obtained for 260-nm thick HfO_2 e-beam evaporated films reported in the literature, indicating that the layer could have reached a low level of porosity of around 9.4% [55]. In this regard, the porosity of coatings deposited by direct evaporation, EBE and IBS techniques has been thoroughly studied [56]. In those studies, it has been demonstrated that the utilisation of plasma or ion assistance during the depositions produced an improvement of the coating densities towards the bulk material, resulting in larger refractive index, better mechanical and structural properties. The studies also showed that IBS produces more compact films, with higher refractive index compared to EBE and hence less porosity. The low stress obtained in PA-EBE coatings deposited here, indicates the benefit of the plasma assistance to reduce the porosity and improve both mechanical and optical properties.

3.6 Coating mechanical loss

Table 3 shows the resulting mechanical loss angles measured by GeNS system (Fig. 3(a)), including substrate ($\phi_{substrate}$) and coated (ϕ_{coated}) loss obtained from ringdown measurements (Fig. 3(b)) and Eq(1). The table also includes the coating ($\phi_{coating}$) loss calculated by using the substrate/coating energy ratio (E_s/E_c) obtained in ANSYS and Eq(2). An extended version of this table including results obtained in a second GeNS system available at University of Strathclyde (UoS) could be found in the supplementary information (*see* Section D) showing a fair agreement with the results showed in Table 3.

Table 3. $\phi_{substrate}$, ϕ_{coated} and $\phi_{coating}$ of single layer coatings for various resonant modes.

Sample (*thickness*)	**Frequency (Hz)**	$\phi_{substrate}$ **(×10^{-6})**	ϕ_{coated} **(×10^{-6})**	E_s/E_c	$\phi_{coating}$ **(×10^{-4})**
Sc_2O_3 (*396 nm*)	556	1.82 ± 0.02	4.26 ± 0.03	169.41	4.1 ± 0.1
	1277	2.15 ± 0.04	6.39 ± 0.06	170.39	7.22 ± 0.06
	3387	1.83 ± 0.05	6.89 ± 0.04	163.60	8.3 ± 0.1
	4786	1.93 ± 0.03	5.32 ± 0.03	162.50	5.5 ± 0.1
MgF_2 (*345 nm*)	549	1.73 ± 0.03	8.23 ± 0.03	275.65	17.92 ± 0.07
	1266	1.41 ± 0.03	9.35 ± 0.03	280.79	22.29 ± 0.06
	4763	1.35 ± 0.02	8.15 ± 0.03	269.56	18.30 ± 0.01
HfO_2 (*238 nm*)	513	1.01 ± 0.05	7.13 ± 0.04	314.29	19.2 ± 0.3
	1189	1.95 ± 0.04	4.25 ± 0.01	308.68	7.1 ± 0.2
	2076	2.72 ± 0.03	6.25 ± 0.05	304.85	10.8 ± 0.1
	3132	1.86 ± 0.02	5.37 ± 0.03	307.82	10.8 ± 0.2

For the sake of clarity, the $\phi_{substrate}$, ϕ_{coated} and $\phi_{coating}$ loss angles summarised in Table 3 are also presented in Fig. 6 (a). In that figure, it is observed the low loss exhibited by the silica substrates (blue triangles) after their annealing at 1000 ºC (releasing any accumulated stress). The figure also shows ϕ_{coated} for the three materials in the range of 10^{-6}. Subtracting the effect of the substrate, and considering the E_s/E_c energy ratio (Eq(2)), one could obtain the $\phi_{coating}$. The low $\phi_{coating}$ values of 4.1×10^{-4} obtained in Sc_2O_3 films make the evaporation method used here to be promising a technique for high index Sc_2O_3 based coatings (Fig. 6 (a)). All the coatings show an approximate constant dependence of the $\phi_{coating}$ with respect to the resonant frequency. Among all, MgF_2 is the coating exhibiting $\phi_{coating}$ in the range of 10^{-3} (Fig. 6 (b)). MgF_2 coatings deposited by different techniques showed $\phi_{coating}$ of $(5.5\text{-}7.5)\times10^{-4}$ at 2.5-39 kHz (IBS technique) [13] and $(3.5\text{-}5.0)\times10^{-4}$ at 30 Hz (thermal evaporation) [57] which highlights the different nature of the resulting thin films grown with a different technique.

Fig. 6 (c) presents high $\phi_{coating}$ for HfO_2 ranged between $(7\text{-}19)\times10^{-3}$. In contrast, IBS HfO_2 coatings presented lower loss values ranged between $(0.9\text{-}1)\times10^{-3}$ and even lower when coatings were subjected to annealing treatments as it will be discussed later on [36].

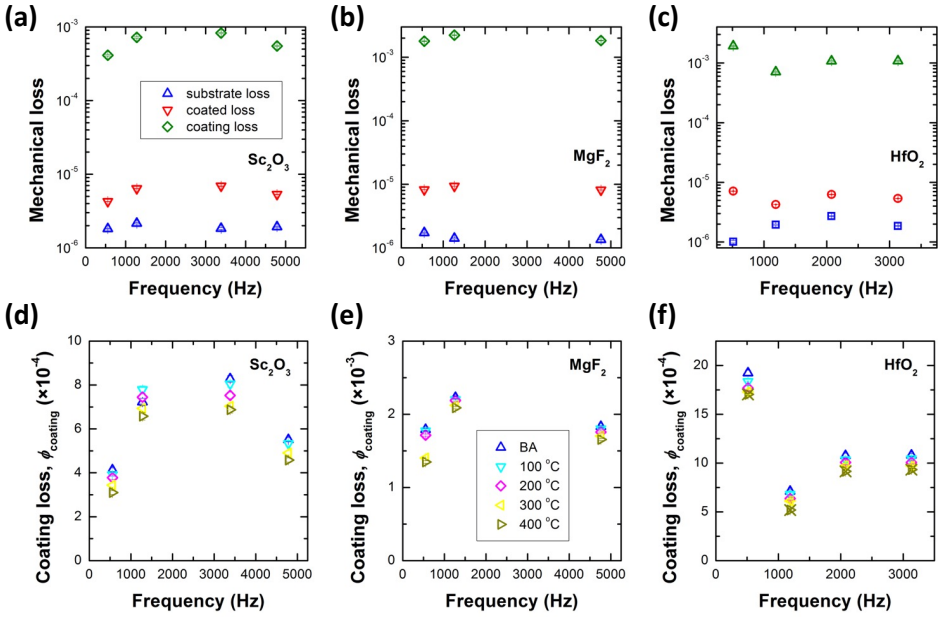

Fig. 6. (a-c) Substrate, coated sample and coating mechanical loss angle of (a) Sc_2O_3, (b) MgF_2 and (c) HfO_2 dielectric materials measured at RT. (d-f) Coating mechanical loss ($\phi_{coating}$) angle of (d) Sc_2O_3, (e) MgF_2 and (f) HfO_2 dielectric materials measured BA and after different annealing treatments ranged between 100 and 400ºC (for 2 hours).

Those $\phi_{coating}$ could be further reduced by the application of thermal annealing below the crystallisation temperature [1] [36], and the optimisation of the evaporation conditions (mainly through the increase of the ion energy and reduced deposition rate). As such, coating loss was measured for each material after various thermal treatments carried out for 2 hours at 100, 200, 300, and 400 ºC. The results of the experiment are summarised in Fig. 6 (d-f) with outcomes from the annealing study resulted in a beneficial impact on all coating losses. It is observed in Fig. 6 (d-f) how the loss angle decreases as the temperature of the annealing increases. This provides indirect evidence of the reduction of defects density within the structure of the coatings, preventing the dissipation of the energy during the Q-factor measurements. Analysing case by case, it is found that for the Sc_2O_3 coating, the fundamental mode, showing the minimum $\phi_{coating}$ of 4.1×10^{-4} further reduced its value down to 3.05×10^{-4} after an annealing treatment of 400ºC for 2 hours. Annealing treatments in MgF_2 coatings did produce a reduction of the $\phi_{coating}$ in all the modes under analysis, however, their values were still in the 10^{-3} range (Fig. 6 (e)). Finally, HfO_2 exhibited a drastic reduction of $\phi_{coating}$ due to the thermal effects brining the $\phi_{coating}$ down to 4×10^{-4} (Fig. 6 (f)) which is close to the 3×10^{-4} reported for RBTD HfO_2 annealed at 650 ºC for 10 hours (0.3×10^{-4}) [12], but till one order of magnitude higher than those reported for IBS HfO_2 coatings annealed at 400 ºC for 24 hours [36]. However, although the HfO_2 presents a very low mechanical loss (lower than most of the h-index metal oxides proposed by GWDs) its high Young's modulus values are four times higher than that of SiO_2. This dissimilar Young's modulus values between substrate (SiO_2) and coating is expected to lead to increased thermal noise [12].

3.7 Optical properties

T and R spectra (Fig. 7 (a)) have been used to calculate refractive index (n) of coatings as a function of the wavelength using the Sellmeier expression (Fig. 7 (b)). Results obtained at λ = 1064 nm show n of 1.75 (Sc_2O_3), 1.33 (MgF_2) and 1.89 (HfO_2). The extinction coefficient in the evaporated films is below the detection limit of the spectrophotometer instrument over the wavelength range of inspection (measurable extinction coefficients higher than 10^{-3}). Further optimisation of n needs to be performed through increased plasma source outpution energy during the evaporation process [4, 12].

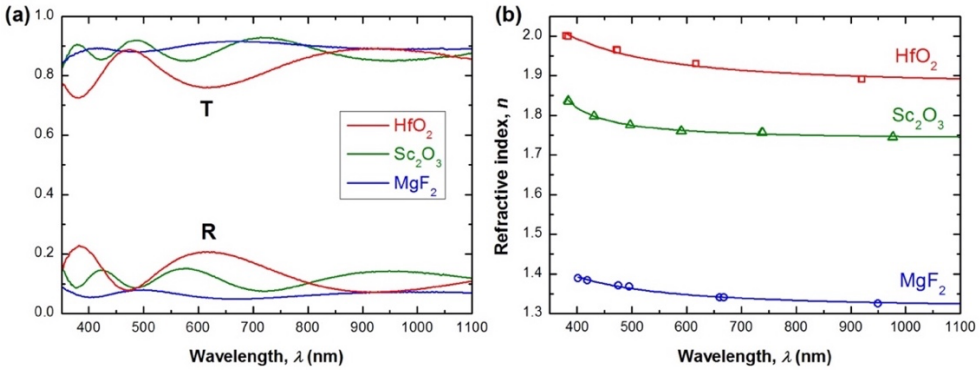

Fig. 7. (a) T and R, and (b) n of Sc_2O_3, MgF_2 and HfO_2 thin films vs wavelength.

Table 4 compares the optical constants obtained here (Fig. 7 (b)) with those reported in the literature. HfO_2 showed a high index of 1.89 in a good agreement with those results obtained with the same technique [59] and slightly lower than those reported by PIAD (1.95) [45] and IBS (2.09) [12][44]. In the case of PIAD, the optimisation of the applied voltage during the deposition process benefited to the resulting optical constant, similarly to the effects on the absorption (as it will be described later on). Among the three, IBS showed the highest refractive index which evidences a more compact and less porous structure, close to the bulk HfO_2 material.

Sc_2O_3 films presented a moderated high index still far from those reported by sputtering systems such as IBS (1.95) [46] and RMS (1.91-1.97)[60], the latter highly subjected to changes in the stoichiometry of the Sc_xO_y film. Based on that report, and using the evidence extracted from EDX analysis (*see* Table 2), the EBE process needs to be optimised in order to improve the stoichiometry of the films, improving the optical properties.

As showed in Table 4, MgF_2 PA-EBE in this work, showed lower refractive index than IBS (1.405), IBAD (1.37-1.44), and thermal evaporation (1.42) techniques. This result points out the differences between coatings deposited by different techniques (nature of the method) and offers a promising alternative for the low-index film in the GWDs.

Table 4. Refractive index of the HfO_2, Sc_2O_3, and MgF_2 coatings (*pristine samples*) deposited by EBE, compared to the literature.

Material	**Refractive index, n (@ λ = 1064 nm)**	
	EBE (*this work*)	Others
HfO_2	1.89 ± 0.02	1.88 (EBE) [59] 1.95 (PIAD) [45] 2.09 (IBS) [12]
Sc_2O_3	1.75 ± 0.03	1.95 (IBS) [46]

		1.91-1.97 (RMS) [60]
MgF_2	1.33 ± 0.03	1.42 (evaporation) [37] 1.405 (IBS) [13] 1.30-1.38 (KMS) [61] 1.37-1.44 (IBAD) [62]

EBE: electron beam evaporation; **IBS**: ion beam sputtering; **RMS**: reactive magnetron sputtering; **IBAD**: ion-beam assisted deposition; **KMS**: keep-molecules sputtering

Optical constants have been also analysed as a function of the annealing treatments (Fig. 8). The results presented in Fig. 8(a-c) correspond to the fit to visible wavelength reflectance spectra for single layer coatings on silicon wafer substrate. Refractive index data was obtained using the envelope method and then fit to a 2-oscillator Sellmeier model. The experimental method and the model used here could show slight differences with respect to the dispersive curves presented in Table 4 due to the use of different substrate (glass), and R and T measurements. In this regard, the results discussed in this section will be compared between each other to find the influence of the temperature on the optical constants.

A closer inspection of wavelengths around 1064 nm shows interesting effects of the annealing on the optical properties of the coatings. For example, in the particular case of Sc_2O_3 (Fig. 8(d)), the refractive index increases with the temperature reaching values around 1.958 which are higher than those reported for IBS and close to record values reported for RMS (*see* Table 4). MgF_2 coatings showed a reduction from 1.35 down to 1.31 (Fig. 8(e)), being greatly beneficial to reduce the number of bi-layers in mirror coatings of GWDs. These values are extremely low compared to those obtained by other technique such as IBAD and evaporation, and close to the record values showed by KMS (*see* Table 4). Finally, the results obtained for HfO_2 evidence a high dependence of n with respect to the annealing temperature (Fig. 8(f)). The best results were observed at temperatures of 100ºC, where the n reached the maximum values of 1.908. Higher temperatures were demonstrated to produce a negative impact on the refractive index.

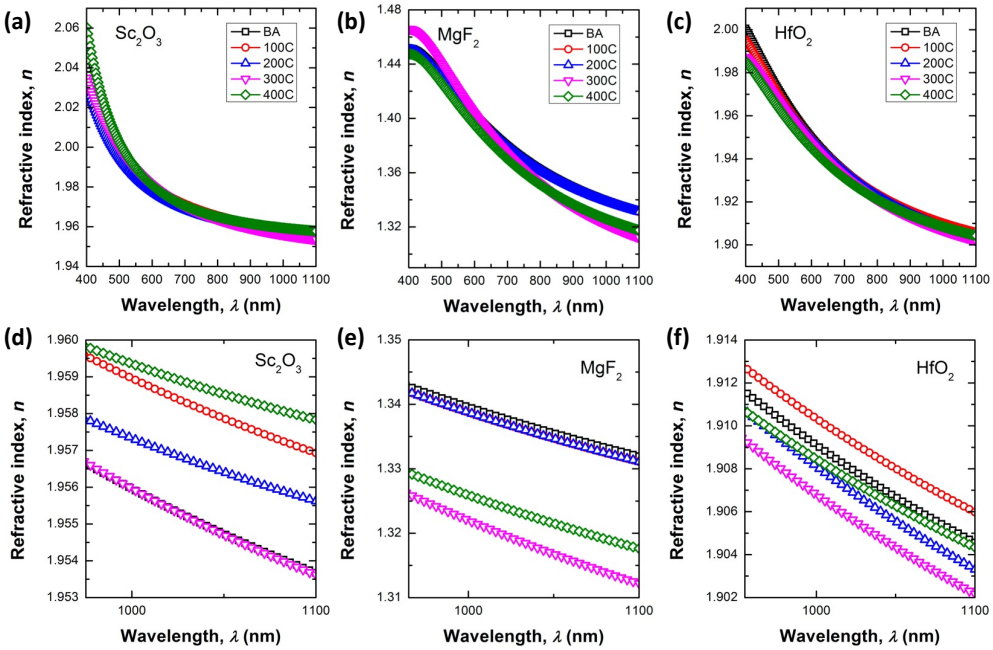

Fig. 8. Refractive index of Sc_2O_3, MgF_2 and HfO_2 obtained Before Annealing (BA) and under different annealing treatments carried out at 100, 200, 300 and 400 ºC.

The variations of the refractive index observed in Fig. 8 were compared against the thickness obtained also from the fitting. Fig. 9 shows the thickness of each coating, including Sc_2O_3 (Fig. 9(a)), MgF_2 (Fig. 9(b)), and HfO_2 (Fig. 9(c)) obtained BA and after annealing treatments carried out for 2 hours at temperatures ranged between 100 and 400 ºC. The study of Sc_2O_3 coating evidences a clear decrease of the thickness from 396 to 356 nm, which is around a 10% reduction with respect to the BA coating thickness. This result indicates an increase of the film compactness, being in good agreement with the increase of the refractive index presented in Fig. 8(a,d). In the case of MgF_2 coating, due to the opposite behaviour observed in the *n* vs temperature curves measured at lower and higher wavelengths Fig. 8(b), it is hard to extract conclusions from Fig. 9(b). In contrast, HfO_2 presents a similar trend than that exhibited by Sc_2O_3, with a reduction of the thickness as the annealing temperature increases (Fig. 9(c)). That reduction was estimated to be lower than in the case of Sc_2O_3 (only 2.5%), but it is in good agreement also with the results presented in Fig. 8(f), where lower temperatures resulted in higher refractive index (i.e., more compact film) than those observed at higher temperatures (less dense films).

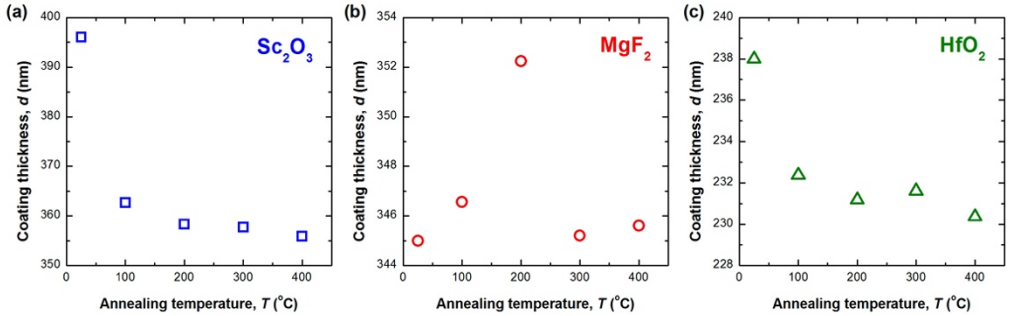

Fig. 9. (a) Sc_2O_3, (b) MgF_2 and (c) HfO_2 coating thickness vs annealing temperature.

Absorption measurements have been carried out on Sc_2O_3, HfO_2 and MgF_2 samples at 1064nm using PCI (Fig. 10). The colour line shows the absorption signal expressed in ppm for scanning the position of the coating through the beam crossing point at which the absorption signal reaches a maximum. These absorption measurements are known as 'z-scans', i.e., translating the coating thickness/sample through the interaction region between respective waists of the pump and probe lasers [63], [64]. The magnitude of the maximum in the absorption scan i.e., the central peak is then directly the optical absorption in ppm presented in Fig. 10. For Sc_2O_3, HfO_2 and MgF_2 coatings deposited in this work, that maximum is found at 16 ± 2, 26.0 ± 0.4, and 840 ± 80 ppm, respectively. The width of the main peak results from the spatial resolution of the PCI system. The small side maxima observed in the graph correspond to interference fringes characteristic for PCI measurements.

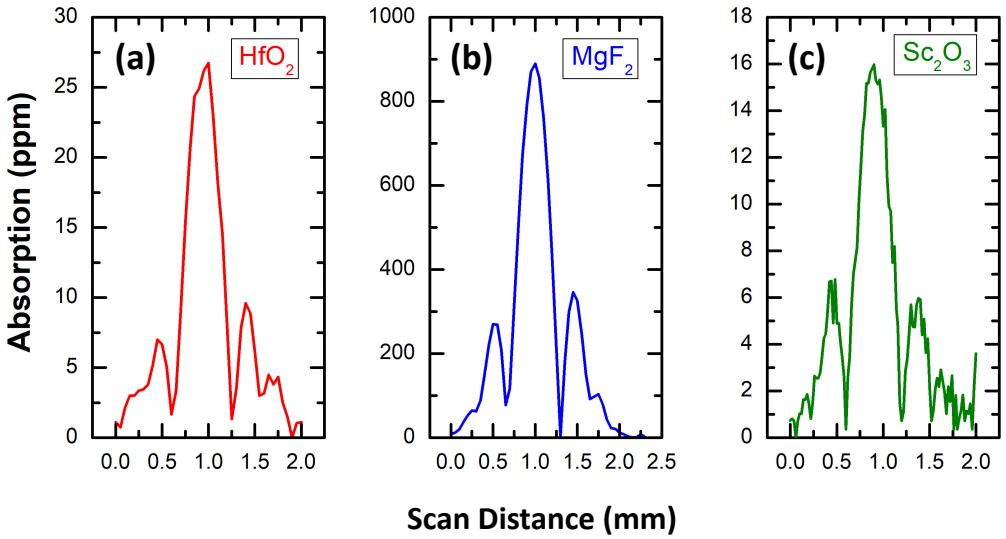

Fig. 10. PCI measurements of the (a) HfO_2, MgF_2 and Sc_2O_3 optical coatings.

The mean value for the absorption of measurements taken at different positions on the disc is summarised in Table 5. That table also presents a comparison with absorption values measured in similar coatings but deposited using other techniques. From the comparison, one could conclude that our coatings showed slightly higher absorption than other deposited by PIAD or IBS. In the particular case of HfO_2, standard deposition of coatings using PIAD at lower applied voltages below 140 V, showed absorptions close to 30 ppm. The increase of the applied voltage above 140 showed a decrease of the absorption down to 13 ppm (with an increase of the refractive index around 2) [45]. That strategy is a promising route also applicable in our deposition technique to further improve the optical properties of the coatings.

Sc_2O_3 coatings deposited in this work exhibited values of absorption of around 16 ppm, which are lower than those obtained by IBS techniques [46]. For the case of MgF_2, the PA-EBE used here needs further optimisation since the absorption of around 840 ppm is three orders of magnitudes above the requirements of current and future GWDs, making this low-index material to be not viable as optical coating. It is also worth noting, that k is 2.1×10^{-4} which is close to that obtained in MgF_2 coatings deposited by IBS technique [13]. Moreover, the k values are three orders of magnitudes larger than that of as-deposited silica layers of current GWDs. For those reasons, further optimisation of the deposition conditions, and characterisation of the coatings not only at 1064 nm, but also at 1550 and 2000 nm, is needed and will be relevant for future GWDs. Moreover, PCI measurements will be performed in

annealed coatings in order to understand better the observed variations in the film thickness, packing density and optical constants with the annealing temperature [65], [66].

Table 5. Absorption and extinction coefficient of Sc_2O_3, MgF_2 and HfO_2 coatings (pristine samples) measured by PCI.

Material	**Absorption (ppm) @ λ = 1064 nm**		**Extinction coefficient, k (10^{-5}) @ λ = 1064 nm**	
	This work	Others	This work	Others
HfO_2	26.0 ± 0.4	13-30 (PIAD) [45]	1.00 ± 0.02	-
Sc_2O_3	16 ± 2	18 (IBS) [46]	0.37 ± 0.02	0.001 (RMS) [60]
MgF_2	840 ± 80	-	21 ± 2	32 (evaporation) [37] 10.62 (IBS) [13]

IBS: ion beam sputtering; **PIAD**: plasma ion-assisted deposition; **RMS**: reactive magnetron sputtering.

4. Conclusions

Sc_2O_3, MgF_2 and HfO_2 films were deposited by ion plasma assisted electron beam evaporation, showing tensile stress of 32, 115 and 150 MPa, significantly lower than coatings deposited by IBS. SEM confirmed the lack of crystalline aggregates and other defects which are the main responsible in IBS coatings increasing the film stress. EDX evidenced that PA-EBE produced non-stoichiometric coatings, exhibiting oxygen excess in both hafnia and scandia (*over stoichiometric*), and fluor deficit in the magnesium fluoride coating (*under stoichiometric*). The analysis of the crystalline structure by GIXRD confirmed the amorphous properties of all the coatings. Thermal treatment of the Sc_2O_3 and MgF_2 coatings up to 700 ºC did not show relevant crystallization in all the coatings; in contrast, HfO_2 coatings exhibited both (120) and (200) diffraction peaks at temperatures >500ºC. Optical characterisation of the films demonstrates high n of 1.75 and 1.89 for Sc_2O_3 and HfO_2 and low n of 1.33 for MgF_2 comparable to those reported in the literature for similar coatings deposited by IBS. Annealing of the coatings, showed an increase of n in the high index materials and a reduction of this constant for the low index one. The characterisation of $\phi_{coating}$ in those films resulted in values in the range of 10^{-4} (Sc_2O_3) and 10^{-3} (MgF_2 and HfO_2) without the application of any thermal treatment. Upon thermal treatments, coating loss showed a reduction with the temperature, exhibiting best values for all the coatings at 400ºC. Moreover, annealing treatments produced an improvement of coatings optical properties through the increase of n in Sc_2O_3 and HfO_2 coatings up to of 1.959 (400ºC) and 1.908 (100ºC), respectively, and the decrease of the n in MgF_2 films down to 1.315 (300ºC). A further optimisation of the optical and mechanical properties is possible through ion energy enhancement by increasing the acceleration voltage in the plasma ion assisted electron beam evaporation and/or reducing deposition rate. Future steps will also involve PCI measurements in annealed samples and spectrophotometry at 1550 and 2000 nm for the investigation of these coatings as potential h- and low-index material for HR coatings in future GWDs.

Acknowledgments: The authors would like to thank the Science and Technology Facilities Council (STFC, ST/V005626/1) and Carnegie Trust (RIG009277) for financial support. The authors also thank their colleagues within the LIGO Scientific Collaboration for advice and support.

Disclosures. The authors declare no conflicts of interest.

Data availability. Data underlying the results presented in this paper are not publicly available at this time but may be obtained from the authors upon reasonable request.

Supplemental document. See Supplement 1 for supporting content.

5. References

[1] G.M. Harry, H. Armandula, E. Black, D. R. M. Crooks, G. Cagnoli, J. Hough, P. Murray, S. Reid, S. Rowan, P. Sneddon, M. M. Fejer, R. Route, and Steven D. Penn, "Thermal noise from optical coatings in gravitational wave detectors," Appl. Opt. **45**, 1569–1574 (2006).

[2] "LIGO-P2000318-v8: GWTC-3: Compact Binary Coalescences Observed by LIGO and Virgo During the Second Part of the Third Observing Run.", doi: 10.48550/arXiv.2111.03606.

[3] M. Granata, A. Amato, L. Balzarini, M. Canepa, J. Degallaix, D. Forest, V. Dolique, L. Mereni, C. Michel, L. Pinard, B. Sassolas, J. Teillon and G. Cagnoli, "Amorphous optical coatings of present gravitational-wave interferometers," Classical and Quant. Grav. **37**, 095004 (2020).

[4] J. Degallaix, C. Michel, B. Sassolas, A. Allocca, G. Cagnoli, L. Balzarini, V. Dolique, R. Flaminio, D. Forest, M. Granata, B. Lagrange, N. Straniero, J. Teillon, and L.Pinard, "Large and extremely low loss: the unique challenges of gravitational wave mirrors," JOSA A **36**, C85-C94 (2019).

[5] L. Pinard, C. Michel, B. Sassolas, L. Balzarini, J. Degallaix, V. Dolique, R. Flaminio, D. Forest, M. Granata, B. Lagrange, N. Straniero, J. Teillon, and G. Cagnoli, "Mirrors used in the LIGO interferometers for first detection of gravitational waves" Appl. Opt. **56.4**, C11-C15 (2017).

[6] A. Paolone, E. Placidi, E. Stellino, M.G. Betti, E. Majorana, C. Mariani, A. Nucara, O. Palumbo, P. Postorino, M. Sbroscia, and F. Trequattrini, "Argon and Other Defects in Amorphous SiO_2 Coatings for Gravitational-Wave Detectors," Coatings **12**, 1001 (2022).

[7] R. B. Cummings, I. MacLaren, R. Bassiri, and I. W. Martin, "Argon bubble formation in tantalum oxide-based films for gravitational wave interferometer mirrors," Opt. Mater. Express **11**, 707-718 (2021).

[8] C. Harthcock, S. R. Qiu, R. A. Negres, J. A. Hammons, T. Voisin, G. Guss, A. A. Martin, C. J. Stolz, M. G. Menor, G. Bhowmik, and M. Huang, "The impact of nano-bubbles on the laser performance of hafnia films deposited by oxygen assisted ion beam sputtering method," Appl. Phys. Lett. **115**, 251902 (2019).

[9] A. Paolone, E. Placidi, E. Stellino, M.G. Betti, E. Majorana, C. Mariani, A. Nucara, O. Palumbo, P. Postorino, I. Rago, and F. Trequattrini, "Effects of the annealing of amorphous Ta_2O_5 coatings produced by ion beam sputtering concerning the effusion of argon and the chemical composition," J. Non Cryst. Solids **557**, 120651 (2021).

[10] A. Amato, G. Cagnoli, M. Granata, B. Sassolas, J. Degallaix, D. Forest, C. Michel, L. Pinard, N. Demos, S. Gras, M. Evans, A. Di Michele, and M. Canepa "Optical and mechanical properties of ion-beam-sputtered Nb_2O_5 and TiO_2-Nb_2O_5 thin films for gravitational-wave interferometers," Phys. Rev. D **103**, 072001 (2021).

[11] A. Amato, S. Terreni, V. Dolique, D. Forest, G. Gemme, M. Granata, L. Mereni, C. Michel, L. Pinard, B. Sassolas, and J. Teillon, "Optical properties of high-quality oxide coating materials used in gravitational-wave advanced detectors," J. Phys. Mater. **2**, 035004 (2019).

[12] M. A. Fazio, G. Vajente, L. Yang, A. Ananyeva, and C. S. Menoni, "Comprehensive study of amorphous metal oxide and Ta_2O_5-based mixed oxide coatings for gravitational-wave detectors," Phys. Rev. D **105** (2021).
[13] M. Granata, A. Amato, M. Bischi, M. Bazzan, G. Cagnoli, M. Canepa, M. Chicoine, A. Di Michele, G. Favaro, D. Forest, G. M. Guidi, G. Maggioni, F. Martelli, M. Menotta, M. Montani, F. Piergiovanni, and F. Schiettekatte, "Optical and Mechanical Properties of Ion-Beam-Sputtered MgF_2 Thin Films for Gravitational-Wave Interferometers," Phys. Rev. Appl. **17**, 034058 (2022).
[14] M. Fazio, L. Yang, A. Markosyan, R. Bassiri, M. M. Fejer, and C. S. Menoni "Growth and characterization of Sc_2O_3 doped Ta_2O_5 thin films," Appl. Opt. **59.5**, A106-A111 (2020).
[15] O. Stenzel, S. Wilbrandt, C. Mühlig, and S. Schröder, "Linear and Nonlinear Absorption of Titanium Dioxide Films Produced by Plasma Ion-Assisted Electron Beam Evaporation: Modeling and Experiments," Coatings **10**, 59 (2020).
[16] M. Alvisi, G. De Nunzio, M. Di Giulio, M. C. Ferrara, M. R. Perrone, L. Protopapa, and L. Vasanelli, "Deposition of SiO_2 films with high laser damage thresholds by ion-assisted electron-beam evaporation," Appl. Opt. **38**, 1237-1243 (1999).
[17] E. F. Fernández, A. García-Loureiro, N. Seoane, and F. Almonacid, "Band-gap material selection for remote high-power laser transmission," Sol. Energy Mater Sol. Cells, **235**, 111483 (2022).
[18] T. Kurobori, T. Yamakage, Y. Hirose, K. I. Kawamura, M. Hirano, and H. Hosono, "Applications of wide-band-gap materials for optoelectronic functional devices fabricated by a pair of interfering femtosecond laser pulses," JJAP **44**, 910–913 (2005).
[19] D. Grosso and P. A. Sermon, "Scandia optical coatings for application at 351 nm," Thin Solid Films, **368**, 116–124 (2000).
[20] M. C. Cheynet, S. Pokrant, F. D. Tichelaar, and J. L. Rouvìre, "Crystal structure and band gap determination of HfO_2 thin films," J. Appl. Phys., **101**, 054101 (2007).
[21] D. T. Wei, "Ion beam interference coating for ultralow optical loss," Appl. Opt. **28**, 2813-2816 (1989).
[22] C.S. Menoni, E.M. Krous, D. Patel, P. Langston, J. Tollerud, D.N. Nguyen, L.A. Emmert, A. Markosyan, R. Route, M. Fejer, and W. Rudolph, "Advances in ion beam sputtered Sc_2O_3 for optical interference coatings," Laser-Induced Damage in Optical Materials, **7842**, 27–38 (2010).
[23] P. Kong, Y. Pu, P. Ma, and J. Zhu, "Relationship between Oxygen Defects and Properties of Scandium Oxide Films Prepared by Ion-Beam Sputtering," Coatings, **9**, 517 (2019).
[24] A. Belosludtsev, K. Juškevičius, L. Ceizaris, R. Samuilovas, S. Stanionytė, V. Jasulaitienė, and S. Kičas, "Correlation between stoichiometry and properties of scandium oxide films prepared by reactive magnetron sputtering," Appl. Surf. Sci. **427**, 312–318 (2018).
[25] G. A. Govindassamy, J. J. Prentice, J. G. Lunney, R. W. Eason, and J. I. Mackenzie, "Effect of laser repetition rate on the growth of Sc_2O_3 via pulsed laser deposition," Appl. Phys. A Mater. Sci. Process **128** (2022).
[26] C. J. Stolz, F. Rainer, G. E. Loomis, M. R. Kozlowski, R. Chow, and S. Falabella, "Reactive evaporation of low-defect density hafnia," Appl. Opt. **32**, 5567-5574 (1993).
[27] M. Balog, M. Schieber, M. Michman, and S. Patai, "Chemical vapor deposition and characterization of HfO_2 films from organo-hafnium compounds," Thin Solid Films **41**, 247–259 (1977).

[28] Edlou, Samad M., Ali Smajkiewicz, and Ghanim A. Al-Jumaily. "Optical properties and environmental stability of oxide coatings deposited by reactive sputtering." Appl. Opt. **32.28**, 5601-5605 (1993).
[29] A. Smajkiewicz, G. A. Al-Jumaily, and S. M. Edlou, "Optical properties and environmental stability of oxide coatings deposited by reactive sputtering," Appl. Opt. **32**, 5601-5605 (1993).
[30] O. Arnon and P. Baumeister, "Use of hafnium dioxide in multilayer dielectric reflectors for the near UV," Appl. Opt. **16**, 439-444 (1977).
[31] M. Q. Zhan, D. P. Zhang, T. Y. Tan, H. B. He, J. da Shao, and Z. X. Fan, "Optical, Structural and Laser-Induced Damage Threshold Properties of HfO_2 Thin Films Prepared by Electron Beam Evaporation," Chinese Phys. Lett. **22**, 1246 (2005).
[32] J. P. Lehan, Y. Mao, B. G. Bovard, and H. A. Macleod, "Optical and microstructural properties of hafnium dioxide thin films," Thin Solid Films **203**, 227–250 (1991).
[33] D. Blaschke, F. Munnik, J. Grenzer, L. Rebohle, H. Schmidt, P. Zahn, and S. Gemming, "A correlation study of layer growth rate, thickness uniformity, stoichiometry, and hydrogen impurity level in HfO_2 thin films grown by ALD between 100° C and 350° C," Appl. Surf. Sci. **506**, 144188 (2020).
[34] M.S. Lebedev, V.N. Kruchinin, M.Y. Afonin, I.V. Korolkov, A.A. Saraev, Gismatulin, and V.A. Gritsenko, "Optical properties and charge transport of textured Sc_2O_3 thin films obtained by atomic layer deposition," Appl. Surf. Sci. **478**, 690–698 (2019).
[35] A. Vinod, M. Rathore, and N.S. Rao, "Effects of annealing on quality and stoichiometry of HfO_2 thin films grown by RF magnetron sputtering," Vacuum **155**, 339–344 (2018).
[36] M. R. Abernathy, S. Reid, E. Chalkley, R. Bassiri, I. W. Martin, K. Evans, M. M. Fejer, A. Gretarsson, G. M. Harry, J. Hough, I. MacLaren, A. Markosyan, P. Murray, R. Nawrodt, S. Penn, R. Route, S. Rowan and P. Seidel, "Cryogenic mechanical loss measurements of heat-treated hafnium dioxide," Classical and Quant. Grav. **28**, 195017 (2011).
[37] L. Dumas, E. Quesnel, J.-Y. Robic, and Y. Pauleau, "Characterization of magnesium fluoride thin films deposited by direct electron beam evaporation," J. Vac. Sci. & Techn. A **18**, 2 (2000).
[38] K. Kawamata, T. Shouzu, N. Mitamura, "KMS (keep-molecules sputtering) deposition of optical MgF_2 thin films," Vacuum, **51(4)**, 559-564 (1998).
[39] K. H. Guenther, "Microstructure of vapor-deposited optical coatings," Optics **23(21)**, 3806-3816 (1984).
[40] B. Hui, X. Fu, D. Gibson, D. Child, S. Song, L. Fleming, L., G. Rutins, H. On Chu, C. Clark, and S. Reid, "Automated Control of Plasma Ion-Assisted Electron Beam-Deposited TiO_2 Optical Thin Films," Coatings **8**, 272 (2018).
[41] S. W. Hsu, T. S. Yang, T. K. Chen, and M. S. Wong, "Ion-assisted electron-beam evaporation of carbon-doped titanium oxide films as visible-light photocatalyst," Thin Solid Films **515**, 3521–3526 (2007).
[42] D. C. Paine, "Study of the effect of Sn doping on the electronic transport properties of thin film indium oxide," Appl. Phys. Let., **2.11**, 1268-1270 (1993).
[43] D. Child, D. Gibson, F. Placido, and E. Waddell, "Enhanced hollow cathode plasma source for assisted low pressure electron beam deposition processes," Surf. Coat. Technol. **267**, 105-110 (2015).
[44] J. Steinlechner, C. Krüger, I.W. Martin, A. Bell, J. Hough, H. Kaufer, S. Rowan, R. Schnabel, and S. Steinlechner, "Optical absorption of silicon nitride membranes at 1064 nm and at 1550 nm," Phys. Rev. D **96**, 022007 (2017).

[45] J. Shao, K. Yi, M. Zhu, and Z. Fan, "Influence of APS bias voltage on properties of HfO_2 and SiO_2 single layer deposited by plasma ion-assisted deposition," Chinese Opt. Lett. **9**, 023101 (2011).
[46] E.M. Krous, D. Patel, P. Langston, C. S. Menoni, A. Markosyan, R. K. Route, M. M. Fejer, D. Nguyen, L. A. Emmert, and W. Rudolph., "Scandium oxide thin films deposited by dual ion beam sputtering for high-power laser applications," Opt. Inter. Coatings, **FA10** (2010).
[47] E. Cesarini, M. Lorenzini, E. Campagna, Filippo Martelli, Francesco Piergiovanni, Flavio Vetrano, G. Losurdo, and G. Cagnoli., "A 'gentle' nodal suspension for measurements of the acoustic attenuation in materials," Rev. Sci. Inst. **80**, 053904 (2009).
[48] M. Granata, L. Balzarini, J. Degallaix, V. Dolique, R. Flaminio, D. Forest, D. Hofman, C. Michel, R. Pedurand, L. Pinard, and B. Sassolas, "Internal friction and young's modulus measurements on SiO_2 and Ta_2O_5 films done with an ultra-high Q silicon-wafer suspension," Arch. Metall. Mater. **60**, 365–370 (2015).
[49] S.D. Penn, P.H. Sneddon, H. Armandula, J.C. Betzwieser, G. Cagnoli, J. Camp, D.R.M. Crooks, M.M. Fejer, A.M. Gretarsson, G.M. Harry, and J. Hough, "Mechanical loss in tantala/silica dielectric mirror coatings," Classical and Quant. Grav. **20.13**, 2917 (2003).
[50] H.F. McMurdie, M.C. Morris, E.H. Evans, B. Paretzkin, W. Wong-Ng, Y. Zhang, and C.R. Hubbard, "Standard X-Ray Diffraction Powder Patterns from The JCPDS Research Associateship," Powder Diffr. **2**, 41–52 (1987).
[51] L. Dumas, E. Quesnel, J.-Y. Robic, and Y. Pauleau, "Characterization of magnesium fluoride thin films deposited by direct electron beam evaporation," J. Vac. Sci. Tech. A, **18**, 465 (2000).
[52] L. Dumas, E. Quesnel, F. Pierre and F. Bertin, "Optical properties of magnesium fluoride thin films produced by argon ion-beam assisted deposition," J. Vac. Sci. and Tech. A **20**, 102 (2002).
[53] C.S. Menoni, E.M. Krous, D. Patel, P. Langston, J. Tollerud, D.N. Nguyen, L.A. Emmert, A. Markosyan, R. Route, M. Fejer, and W. Rudolph, "Advances in ion beam sputtered Sc_2O_3 for optical interference coatings," Laser-Induced Damage in Optical Materials: **7842**, 784202 (2010).
[54] H. K. Pulker and J. Mäser, "The origin of mechanical stress in vacuum-deposited MgF_2 and ZnS films," Thin Solid Films **59**, 65–76 (1979).
[55] S. Jena, R. B. Tokas, S. Thakur, and D. V. Udupa, "Study of aging effects on optical properties and residual stress of HfO_2 thin film," Optik (Stuttg) **185**, 71–81 (2019).
[56] L. Gallais, J. Capoulade, J.Y. Natoli, M. Commandré, M. Cathelinaud, C. Koc, and M. Lequime, "Laser damage resistance of hafnia thin films deposited by electron beam deposition, reactive low voltage ion plating, and dual ion beam sputtering," Appl. Opt. **47**, C107-C113 (2008).
[57] A. Kinbara, S. Baba, N. Matuda, and K. Takamisawa, "Mechanical properties of and cracks and wrinkles in vacuum-deposited MgF_2, carbon and baron coatings," Thin Solid Films **84**, 205–212 (1981).
[58] M. Fazio, L. Yang, A. Markosyan, R. Bassiri, M. M. Fejer, and C. S. Menoni, "Growth and characterization of Sc_2O_3 doped Ta_2O_5 thin films," Appl. Opt. **59**, A106 (2020).
[59] M. F. Al-Kuhaili, S. M. A. Durrani, and E. E. Khawaja, "Characterization of hafnium oxide thin films prepared by electron beam evaporation," J. Phys. D **37**, 1254 (2004).
[60] A. Belosludtsev, K. Juškevičius, L. Ceizaris, R. Samuilovas, S. Stanionytė, V. Jasulaitienė, and S. Kičas, "Correlation between stoichiometry and properties of

scandium oxide films prepared by reactive magnetron sputtering" Appl. Surf. Sci. **427**, 312-318 (2018).
[61] K. Kawamata, T. Shouzu, and N. Mitamura. "KMS (keep-molecules sputtering) deposition of optical MgF_2 thin films." Vacuum **51.4**, 559-564 (1998).
[62] L. Dumas, E. Quesnel, F. Pierre, and F. Bertin, "Optical properties of magnesium fluoride thin films produced by argon ion-beam assisted deposition," J. Vac. Sci. & Techn. A **20**, 102 (2002).
[63] M. Fletcher, S. Tait, J. Steinlechner, I.W. Martin, A.S. Bell, J. Hough, S. Rowan, and R. Schnabel, "Effect of stress and temperature on the optical properties of silicon nitride membranes at 1,550 nm," Front. Mater. **5** (2018).
[64] F. M. Kiessling, P.G. Murray, M. Kinley-Hanlon, I. Buchovska, T.K. Ervik, V. Graham, J. Hough, R. Johnston, M. Pietsch, S. Rowan, and R. Schnabel "Quasi-monocrystalline silicon for low-noise end mirrors in cryogenic gravitational-wave detectors," Phys. Rev. Res. **4**, 043043 (2022).
[65] T. Tan, Z. Liu, H. Lu, W. Liu, and H. Tian, "Structure and optical properties of HfO_2 thin films on silicon after rapid thermal annealing," Opt. Mater. (Amst.) **32**, 432–435 (2010).
[66] S. B. Khan, Z. Zhang, and S. L. Lee, "Annealing influence on optical performance of HfO_2 thin films," J. Alloys Compd. **816**, 152552 (2020).